Monthly Notices
of the
ROYAL ASTRONOMICAL SOCIETY

MNRAS **489,** 2298–2306 (2019)
Advance Access publication 2019 August 26

doi:10.1093/mnras/stz2360

Interacting young M-dwarfs in triple system – Par 1802 binary system case study

Shelley J. Cheng [1]★ Alec M. Vinson [1] and Smadar Naoz [1,2]

[1] *Department of Physics and Astronomy, University of California, Los Angeles, CA 90095, USA*
[2] *Mani L. Bhaumik Institute for Theoretical Physics, Department of Physics and Astronomy, UCLA, Los Angeles, CA 90095, USA*

Accepted 2019 August 21. Received 2019 August 21; in original form 2019 June 28

ABSTRACT

The binary star Par 1802 in the Orion Nebula presents an interesting puzzle in the field of stellar dynamics and evolution. Binary systems such as Par 1802 are thought to form from the same natal material and thus the stellar members are expected to have very similar physical attributes. However, Par 1802's stars have significantly different temperatures despite their identical (within 3 per cent) masses of about 0.39 $M_{\odot}$. The leading proof-of-concept idea is that a third companion gravitationally induced the two stars to orbit closer than their Roche limit, which facilitated heating through tidal effects. Here we expand on this idea and study the three-body dynamical evolution of such a system, including tidal and pre-main-sequence evolution. We also include tidal heating and mass transfer at the onset of Roche limit crossing. We show, as a proof-of-concept, that mass transfer combined with tidal heating can naturally explain the observed temperature discrepancy. We also predict the orbital configuration of the possible tertiary companion. Finally, we suggest that the dynamical evolution of such a system has pervasive consequences. We expect an abundance of systems to undergo mass transfer during their pre-main-sequence time, which can cause temperature differences.

Key words: binaries: close – binaries: general – stars: kinematics and dynamics – stars: low-mass – stars: pre-main-sequence.

1 INTRODUCTION

Basic physical properties of a star such as mass and temperature are strongly determined by its initial mass and chemical composition. Equal-mass components of binary stars are typically considered to be coeval and identical 'twins' formed from the same protostellar core, and are expected to have identical physical attributes. However, a small number of identical twin systems seem to be inconsistent with this narrative, featuring a large temperature difference between its component stars. These systems are rare, with ∼5 such systems having been observed and studied (e.g. Cargile, Stassun & Mathieu 2008; Gómez Maqueo Chew et al. 2009, 2019; Wang et al. 2009; Gillen et al. 2017). We suggest that this type of system is a natural result of dynamical evolution in three-body systems.

As a case study, we focus on the Par 1802 binary system (Stassun et al. 2008). This system is a relatively young (few million years old; see Cargile, Stassun & Mathieu 2008; Gómez Maqueo Chew et al. 2012; Stassun, Feiden & Torres 2014) pre-main-sequence 'twin' composed of two M-dwarf stars, each with identical (within 3 per cent) masses of 0.391 and 0.385 $M_{\odot}$ (Gómez Maqueo Chew et al. 2012; Stassun et al. 2014). However, the temperatures of the binary stars are 3675 and 3365 K, which surprisingly differ by ∼300 K (or 9.2 per cent; Gómez Maqueo Chew et al. 2012; Stassun et al. 2014) despite their otherwise identical physical attributes.

The majority (∼75 per cent; Salpeter 1955; Henry et al. 2006) of all the stars in our Galaxy are low-mass (about 10–50 per cent the mass of the Sun) and cold (about 30–65 per cent the temperature of the Sun) stars that belong to the M-dwarf (red dwarf) class. Approximately 20–40 per cent of all M-dwarfs have a binary companion (Fischer & Marcy 1992; Bergfors et al. 2010; Raghavan et al. 2010; Janson et al. 2012), and in a survey of 151 contact binaries using data from the *Hipparcos* satellite mission, Pribulla & Rucinski (2006) found that 42 ± 5 per cent are at least in triple systems. Therefore, many binary stars in our Galaxy are in fact in triple configurations (Tokovinin 1997; Tokovinin et al. 2006; Eggleton, Kisseleva-Eggleton & Dearborn 2007; Griffin 2012; Rappaport et al. 2013).

The prevalence of M-dwarf binaries in triple systems motivated Gómez Maqueo Chew et al. (2012) and Stassun et al. (2014) to study Par 1802 in the presence of a third star. In particular, they proposed that the temperature difference between the components of Par 1802 is likely due to different spin evolution and uneven mass accretion, perhaps caused by pre-main-sequence tidal evolution between the two stars. However, their work did not include the dynamical

★ E-mail: shelleycheng@ucla.edu

evolution of the three-body system, which can dramatically alter the binary's orbital parameters (e.g. Naoz 2016). Here we follow the dynamical evolution of a Par 1802-like system and show that a distant tertiary can naturally explain all of the observed properties. Moreover, we constrain the orbital configuration of the third companion.

Dynamical stability of such a system requires a hierarchical configuration where a third body on a far wider (outer) orbit orbits around the tighter (inner) binary of Par 1802. In this configuration, the triple body orbital parameters change on secular time-scales. In particular, gravitational perturbations from the tertiary star can cause eccentricity excitations of the inner orbit, i.e. Kozai–Lidov cycles (Kozai 1962; Lidov 1962; Naoz 2016). The two non-resonant orbits can be described by two 'wires' where the line densities are inversely proportional to orbital velocity. Gravitational potential can then be expanded in the semimajor axial ratio, as the hierarchical configuration drives the ratio between the inner and outer body's semimajor axes to a small parameter. Here, we employ the hierarchical three-body secular approximation up to the octupole level of approximation, known as the eccentric Kozai–Lidov (EKL) mechanism (e.g. Naoz 2016). It was recently shown that the EKL mechanism plays a pivotal role in the evolution of triple stellar systems (Thompson 2011; Naoz et al. 2013a; Naoz & Fabrycky 2014; Naoz 2016; Stephan et al. 2016; Bataille, Libert & Correia 2018; Moe & Kratter 2018). Gravitational perturbations from a third companion excite high eccentricities in the inner binary, thus the stars spend longer times near each other, yielding to stronger tides that can shrink the binary separation and circularizing it. This process is very effective in forming short period inner binaries such as Par 1802 (e.g. Naoz & Fabrycky 2014).

This paper provides a theoretical background (Section 2), describes the set-up for the dynamical simulations (Section 3), presents and analyses results of the simulations (Section 4) with particular emphasis on predictions of the third companion's orbital parameters. We investigate the interaction at Roche limit and explain the observed temperature difference between the stars of the inner binary (Section 5) through a proof-of-concept mass transfer analysis and a tidal heating model. A discussion of our results is offered in Section 6 before drawing our conclusions.

2 THEORY

2.1 Pre-main-sequence evolution

Tidal evolution of such a compact binary system is very sensitive not only to orbital separation, but also to stellar radii. As we are modelling the tidal evolution during the stars' pre-main-sequence lifetime, it is therefore very important to also consider the dramatic evolution in stellar radii during this time. To do this, we consider the calculations of Chabrier & Baraffe (1997) for the radius evolution of small ($<0.8\,M_\odot$) pre-main-sequence stars, wherein they consider stellar evolution as a function of mass and metallicity using grainless non-grey atmosphere models. We interpolate their results, assuming solar metallicity, for pre-main-sequence stars to find radius for each star as a function of its mass and of time while modelling the tidal evolution. The radii of these stars dramatically contracts during their pre-main-sequence lifetime, with initial inflated radii of approximately 11 times the radius of the Sun, to final radii of approximately 1.5 times the radius of the Sun (see Fig. 1). This in turn has dramatic effects on the tidal evolution, with the tidal forces weakening greatly as the star contracts.

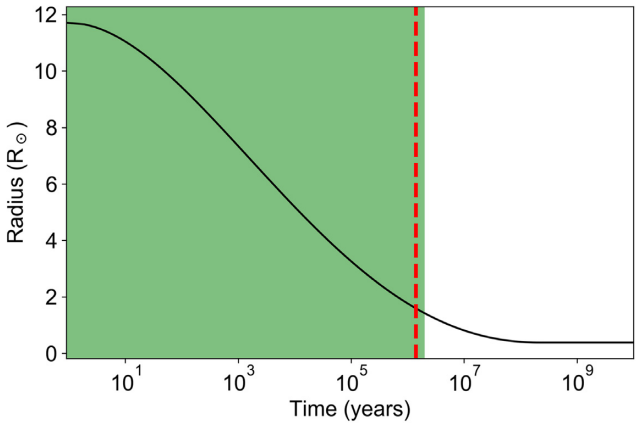

Figure 1. Pre-main-sequence radius contraction for a 0.391 $M_\odot$ M-dwarf star. Interpolated from Chabrier & Baraffe (1997), with pre-main-sequence (and thus radius contraction) ending at 2.1×10^8 yr. The age of the system of ∼2 Myr (Stassun et al. 2014; Gómez Maqueo Chew et al. 2012) is shaded in green. The estimated Roche limit crossing time of 1.4 Myr is in red.

2.2 Analytical expectations for the tertiary companion

Par 1802 is a very tight binary with semimajor axis $a \sim 0.049$ au and on a circularized orbit of eccentricity $e \sim 0.02$ (Gómez Maqueo Chew et al. 2012). The temperature difference between the stars implies that mass transfer may have taken place during Roche limit crossing phase of the evolution. The Roche limit, $R_{\rm Roche,\,1}$, of a body of mass m_1 and radius R_1 with respect to an orbiting body of mass m_2 is defined as

$$R_{\rm Roche,1} = 2.7 \times R_1 \left(\frac{m_1+m_2}{m_1}\right)^{-1/3}. \quad (1)$$

The numerical pre-factor is highly uncertain and here we adopt 2.7 following numerical simulations from Guillochon, Ramirez-Ruiz & Lin (2011) and Liu et al. (2013). As the M-dwarf goes through pre-main-sequence contraction the Roche limit contracts. Thus, a system may have a short phase of mass transfer during the evolution before settling down on a stable tight configuration.

The two stars probably began their life on a wider orbit than currently observed, avoiding merging at birth. The tertiary induces large values of eccentricity that eventually, with tidal evolution, drive the binaries to a tight configuration (e.g. Eggleton, Kiseleva & Hut 1998; Kiseleva, Eggleton & Mikkola 1998; Eggleton & Kiseleva-Eggleton 2001; Fabrycky & Tremaine 2007; Perets & Fabrycky 2009; Thompson 2011; Shappee & Thompson 2013; Naoz & Fabrycky 2014). The final semimajor axis from this process is most likely the result of tidal shrinking that conserved angular momentum (e.g. Ford, Kozinsky & Rasio 2000). In other words, we can write

$$a_{\rm i}\left(1-e_{\rm i}^2\right) \approx a_{\rm f}, \quad (2)$$

where subscript 'i' refers to initial configuration (before tidal effects) and subscript 'f' refers to final configuration, a is the semimajor axis, and e is the eccentricity. High eccentricity migration implies that $e \to 1$ during the evolution, thus

$$a_{\rm f} \sim 2a_{\rm i}(1-e_{\rm i}) \sim 2R_{\rm Roche}, \quad (3)$$

assuming that the closest approach before disruption can be the Roche limit. In our case, where mass transfer may have taken place, $R_{\rm Roche}$ represents the maximum approach for interaction.

Adopting the observed semimajor axis of Par 1802 $a_{\rm f} = 0.049$ au, and using equation (3), we find that the pericentre crosses the Roche

limit at a radius

$$R_1(t) \sim \frac{a_f}{2 \times 2.7} \left(\frac{m_1 + m_2}{m_1} \right)^{-1/3} \sim 1.57\,\mathrm{R}_\odot. \quad (4)$$

We adopt pre-main-sequence evolution of M-dwarfs following Chabrier & Baraffe (1997), and can estimate the time the star reached this value (the vertical line in Fig. 1). We thus estimate that the limit on the Roche limit crossing time was at 1.4×10^6 yr, in other words, about 0.6 Myr ago.

3 THREE-BODY DYNAMICAL EVOLUTION FOR PRE-MAIN-SEQUENCE STARS

Here we discuss the secular three-body evolution in the presence of pre-main-sequence contraction of the stellar radius and general relativity (GR) precession and tides. We begin by describing the EKL evolution and our Monte Carlo implementation. In Section 5.1, we discuss the possibility of mass transfer during Roche limit crossing and calculate the resultant temperature of the stars.

3.1 Three-body dynamical evolution

We study the hierarchical three-body dynamics, tidal, GR, and pre-main-sequence evolution of the binary system Par 1802 in the presence of a tertiary companion. We model the dynamical evolution of these systems by performing Monte Carlo simulations of 7500 different initial systems for 2 Myr, the approximate age of the Par 1802 system (Gómez Maqueo Chew et al. 2012; Stassun et al. 2014). Our Monte Carlo implementation first involves randomly selecting 7500 different sets of initial conditions (that satisfy the stability criteria and constraints described in Section 3.2). We then solve the three-body secular equations up to the octupole level of approximation (following Naoz et al. 2013a) through numerical integration with the Runge–Kutta fourth-order method. We note that a variable step size was used in our numerical integration due to the presence of highly eccentric orbits. Physical processes such as tidal effects and GR precession for the inner and outer orbits (e.g. Naoz et al. 2013b) are included in the numerical integration. Additionally, the effect of shrinking stellar radius during the pre-main-sequence evolution of an M-dwarf, which is of particular interest to the case of the Par 1802 binary, is included in the numerical integration.

The quadrupole level of approximation time-scales for such a system is

$$t_k \sim \frac{16}{15} \frac{\sqrt{m_1 + m_2}}{\sqrt{G} m_3} \frac{a_2^3}{a_1^{3/2}} \left(1 - e_2^2\right)^{3/2}, \quad (5)$$

where G is the gravitational constant, a_1 (a_2) is the inner (outer) semimajor axis, and e_1 (e_2) is the inner (outer) eccentricity. The tidal evolution of the inner binary is determined following Eggleton & Kiseleva-Eggleton (2001) through differential equations that account for distortion due to both tides and rotation. Tidal dissipation follows the equilibrium tidal model in Eggleton et al. (1998), with viscous time-scale $t_V = 0.5$ for all simulations (see Naoz 2016, for full set of equations). This is a simplified treatment of tidal effects as t_V is expected to vary with stellar radius and mass. However, the dependence of t_V on radius and mass is unknown. The apsidal motion constant (which is twice the Love parameter) for this polytrope is 0.014. Hence, this tidal evolution approach is adopted in our integration since it is self-consistent with the secular framework, accounts for precession due to tidal torques and oblateness, and enables us to qualitatively understand the physical effect of tides in the inner binary.

While we adopted equilibrium tides, dynamical tides were shown to have significant effect on the orbital evolution (see for review Mathis 2019). For example, in a fully convective M-type star such as Par 1802, dynamical tides in the convection zone result in a frequency-dependent tidal dissipation (e.g. Greenberg 2009; Vick & Lai 2018) that, at resonances, may be significantly larger than equilibrium tide dissipation (Braviner & Ogilvie 2015). Dynamical tides have numerous potential consequences on dynamical evolution (Witte & Savonije 2002; Auclair-Desrotour, Mathis & Le Poncin-Lafitte 2015), such as causing the binary orbit to rapidly circularize, abrupt shrinking of a, and changes to the orbital period. However, we stress that the equilibrium tide model may capture the qualitative behaviour of the system (e.g. Vick & Lai 2018).

3.2 Initial conditions

The numerical set-up incorporates data from observations of Par 1802, selects initial distributions for unknown orbital quantities, and finally applies constraints and stability criteria. The masses of the constituent stars of Par 1802 (m_1, m_2) are taken to be 0.391 and 0.385 $\mathrm{M}_\odot$ from Gómez Maqueo Chew et al. (2012), and the radii (R_1, R_2) taken to be 11.71 and 11.64 $\mathrm{R}_\odot$, respectively, from Baraffe et al. (1998). The stellar spins for both stars in the inner binary are taken to be 2 d, and the spin–orbit angle was randomly sampled from a uniform distribution. The mass of the third outer star m_3 was randomly sampled from a uniform distribution between 0.1 and 0.8 $\mathrm{M}_\odot$.

The eccentricity of the inner (outer) orbit e_1 (e_2) were sampled from a thermal distribution between 0 and 1. The inclination i between the inner and outer orbit's angular momenta was assumed to be isotropic (i.e. uniform in cosine). The period of the inner and outer orbit was assumed to be the lognormal distribution of Duquennoy & Mayor (1991). Note that this period distribution represents the final periods of binaries population, rather than the initial one. However, if we extrapolate for a recent study for more massive stars, the final period distribution, at wide orbits, is a signature of the birth distribution (Rose, Naoz & Geller 2019).

We also adopt the following stability criteria. The first represents the relative importance of the octupole and quadrupole terms in the system's Hamiltonian (Naoz 2016):

$$\epsilon = \frac{a_1}{a_2} \frac{e_2}{1 - e_2^2} < 0.1. \quad (6)$$

The second stability criterion follows Mardling & Aarseth (2001):

$$\frac{a_2}{a_1} > 2.8 \left(1 + \frac{m_2}{m_1 + m_2}\right)^{2/5} \frac{(1 + e_2)^{2/5}}{(1 - e_2)^{6/5}} \left(1 - \frac{0.3i}{180^\circ}\right). \quad (7)$$

Equation (6) is numerically similar to this criterion (Naoz et al. 2013a). It is noted that the dynamics of systems in the upper limit of equation (6) may be dominated by effects other than the EKL mechanism, especially for a strong perturber (Antonini, Murray & Mikkola 2014; Bode & Wegg 2014). Our work does not take these cases into account because equations (6) and (7) are numerically very close, and therefore it is expected that the vast majority of stable systems can be faithfully described by the EKL mechanism. We also note that these stability criteria deem a system unstable if at any point in time it violates the stability criteria, but do not provide a time-scales for growth of the instability (e.g. Mylläri et al. 2018). In practice we expect more systems to be stable for 2 Myr of our integration time-scales than considered here.

Additionally, we require the pericentre distance to be greater than initial Roche limit, which ensures that the inner binary does

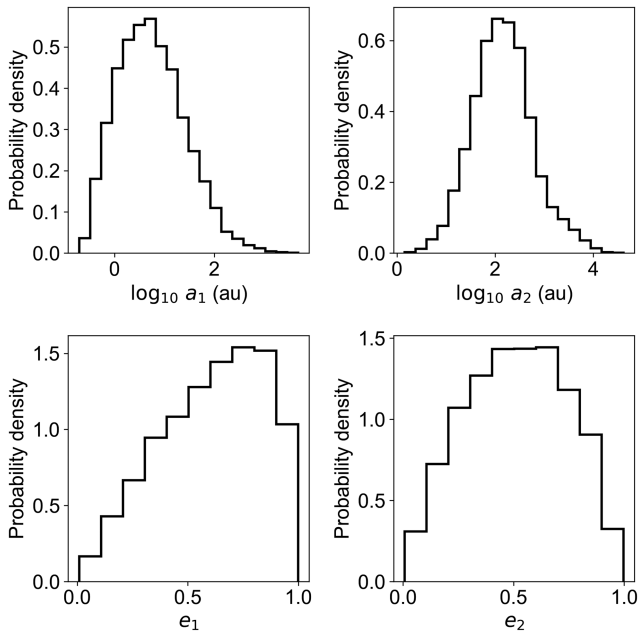

Figure 2. Initial conditions for semimajor axes and eccentricities. The left- and right-hand columns show the distribution of a and e of, respectively, the inner and outer binary. Dynamical stability criteria (see text) are accounted for in these distributions.

not merge before the tertiary companion can affect the system:

$$a_1(1 - e_1) > R_{\mathrm{Roche},1}. \quad (8)$$

Together, these constraints and stability criteria allow us to model systems in which the EKL mechanism may facilitate tidal heating during the pre-main-sequence evolution of the system. We depict the initial conditions of the system in Fig. 2, after these criteria have been applied.

4 THREE-BODY EVOLUTION RESULTS

4.1 Inner orbit dynamical outcomes

We identified two general dynamical outcomes. As expected, the outcome is dependent on the presence and strength of eccentricity excitations. EKL in the presence of tides tends to circularize and tighten systems. Larger eccentricity excitations, due to the EKL mechanism, result in a more efficient production of such systems. The different dynamical outcomes are depicted in Fig. 3, and are summarized in Fig. 4. In the latter figure we consider the initial distribution of a_1 (top) and e_1 (bottom) and overplot the 15 per cent of systems that crossed their Roche limit at any point throughout the 2 Myr evolution (blue line). The green vertical lines in Fig. 4 represent the observed parameters for Par 1802. We then use the observed a_1, up to a factor of 2, to constrain the orbital parameters of the third companion.

4.1.1 Roche limit crossing systems

About 15 per cent of all systems crossed their Roche limit. We identify two subtypes of Roche limit crossing systems.

(i) *Single eccentricity excitation.* Depicted in top left-hand panel of Fig. 3. These systems are in the most efficient part of the parameter space of EKL. Here, the eccentricity undergoes a single dip throughout the evolution, with pericentre dipping below the Roche limit of the inner binary for a time Δt and then exiting the Roche limit. Mass transfer may occur within the Roche limit (see Section 5.1). These systems are of interest since Par 1802 is observed to be circularized ($e_1 = 0.0166$) with small semimajor axis ($a_1 = 0.0496$ au; Gómez Maqueo Chew et al. 2012).

(ii) *Long-term eccentricity oscillations.* Depicted in top right-hand panel of Fig. 3. In these systems EKL oscillations take place, but the eccentricity excitation is not high enough to cause the system to quickly circularize. Tides may cause an increase of a_1. In general, for these systems the inner binary does not circularize and tighten, and therefore these systems are not of interest as they do not match observations.

4.1.2 Non-Roche limit crossing systems

In many cases, the EKL eccentricity excitation is either taking place on longer time-scales than the age of the system (e.g. bottom right-hand panel of Fig. 3), or had not yet reached high eccentricity values (bottom left-hand panel of Fig. 3). These systems are not of interest since the inner binary does not circularize or tighten, and its final configuration does not match observations.

4.2 Tertiary predictions

We focus on Roche limit crossing systems since their behaviour matches the observations of Gómez Maqueo Chew et al. (2012) in which the inner binary is circularized and tightened. We show in Fig. 4 that the vast majority of Roche limit crossing systems (those with a single eccentricity excitation) have a final inner binary configuration that is circularized and tightened. Qualitatively, we note that these systems should be a generic result of the EKL evolution. About 10 per cent of all systems that cross their Roche limit are within in a factor of 2 of Par 1802 observed semimajor axis of 0.0496 ± 0.0008 au and have a circularized orbit. We use this subset to constrain the parameter space for the Par 1802 hypothetical companion. We choose to constrain our predictions using a factor of 2 due to the uncertainties of our model, such as in the pre-factor of the Roche limit in equation (1) and the choice of our viscous time-scales in Section 3.1.

We predict the median semimajor axis for Par 1802 outer binary to likely be 350 au.

As shown in the top panel of Fig. 5, Roche limit crossing systems (blue) have a_2 that ranges between 2 and 2500 au with a median of 55 au. This is distinctly different from the distribution for a_2 for all simulated systems (black), which has a median of 140 au. Because of the young age of Par 1802 (and thus the short time of simulation), the final distribution for a_2 for all systems (black) closely resembles the initial conditions (e.g. top right-hand panel of Fig. 2). This result is consistent with the result for massive stars found by Rose et al. (2019).

The Par 1802-like systems (the 10 per cent of systems within factor of 2 of the observed a_1) have a bimodal distribution in a_2. The low value a_2 peak (median of $\sim$5 au) corresponds to low e_2 systems. The higher a_2 values represent the majority of systems and have a median of $\sim$375 au.

As expected the final distribution of e_2 resembles the initial distribution. The eccentricity of Par 1802-like system's outer orbit corresponds to the outer orbit semimajor axis, with the rule of thumb that lower eccentricity requires lower (closer in) semimajor axis values. The median eccentricity in this case is 0.5 (bottom panel of Fig. 5).

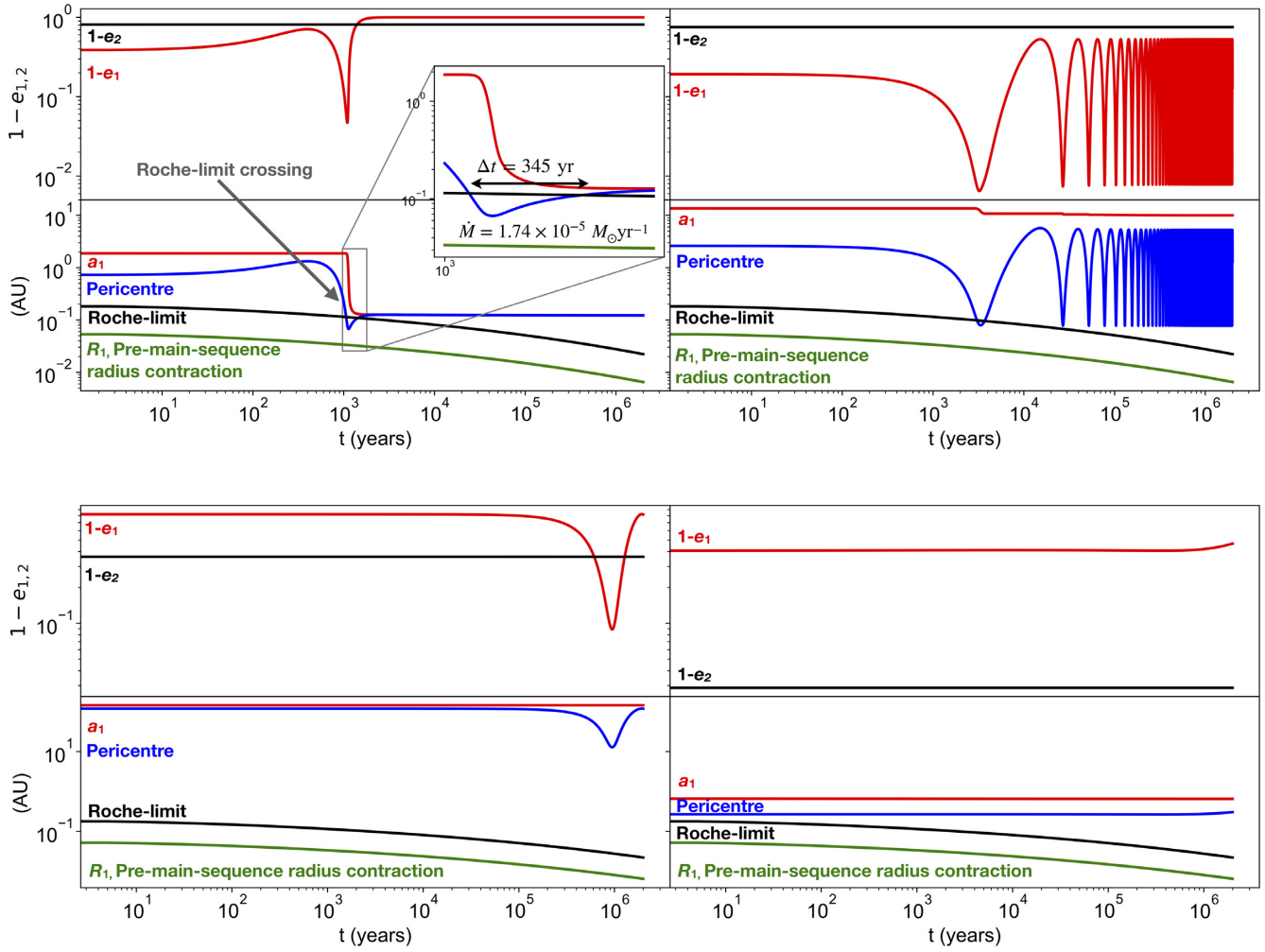

Figure 3. Archetypal systems. We show the time evolution of four triple systems. In the top row, we show two Roche limit crossing systems: with a single eccentricity excitation (left), and with long-term eccentricity oscillations (right). In the bottom row, we show two non-Roche limit crossing systems. For each of the four systems, the top panel shows $1 - e$ of the inner and outer binary, and the bottom panel shows the inner semimajor axis, pericentre, the Roche limit, and R_1, the radius of the more massive inner binary star. When plotted, R_2 is visually indistinguishable from R_1 and is therefore omitted from the figure. All systems have $m_1 = 0.391$ M$_\odot$, $m_2 = 0.385$ M$_\odot$, and spins of 2 d. The initial conditions are (from left to right on top row, then left to right on bottom row): $m_3 = 0.25$, 0.36, 0.67, and 0.49 M$_\odot$, $a_1 = 1.87$, 13.4, 144, and 0.658 au, $a_2 = 14.7$, 108, 2220, and 1195 au, $e_1 = 0.62$, 0.81, 0.18, and 0.59, $e_2 = 0.19$, 0.25, 0.64, and 0.97, $g_1 = 131.^\circ6$, $231.^\circ8$, $263.^\circ5$, and $128.^\circ1$, $g_2 = 136.^\circ0$, $123.^\circ9$, $255.^\circ3$, and $37.^\circ29$, and $i = 86.^\circ4$, 101°, 112°, and 121°.

The inclination of the system (top panel of Fig. 6) also behaves as expected, and we find a bimodal distribution (consistent with Fabrycky, Johnson & Goodman 2007; Naoz & Fabrycky 2014). However, due to the short time-scales of the integration, the bimodal distribution is more closely located near 90° rather than near the Kozai angles, being centred at about 70° and 110°. The inclination of the system is correlated with ϵ (bottom panel of Fig. 6), a parameter that describes the strength of the EKL mechanism. As expected, the EKL mechanism is efficient for systems that cross the Roche limit and particularly efficient for Roche limit-crossing systems that are within a factor of 2 of the observed a_1.

5 INTERACTION AT ROCHE LIMIT

5.1 Mass transfer

At the Roche limit, mass transfer occurs. As a proof-of-concept we assume a conservative mass inversion where the binary mass

$$m_1 + m_2 = 0.776\,\mathrm{M}_\odot = \text{constant}, \tag{9}$$

and that mass transfer only occurs while the inner binary stars are within the Roche limit. We note that Eggleton (1983) adopted the Roche lobe radius (where a surface mass element of a star becomes unbound) as the criterion for mass transfer, with mass transfer occurring slightly earlier. Here, we instead adopt the Roche limit as the criterion for mass transfer, which is more conservative (smaller Δt) than the Roche lobe radius criterion by a small factor of ∼1.2. This factor is well within the uncertainties in the model, and therefore will not lead to any significant qualitative changes to the result.

Thus, the mass transfer rate is loosely defined as

$$\dot{M} = \frac{\Delta M}{\Delta t}, \tag{10}$$

where $\Delta M = m_1 - m_2$. In our proof-of-concept model, the mass transfer rate varies for different lengths of time Δt spent within the

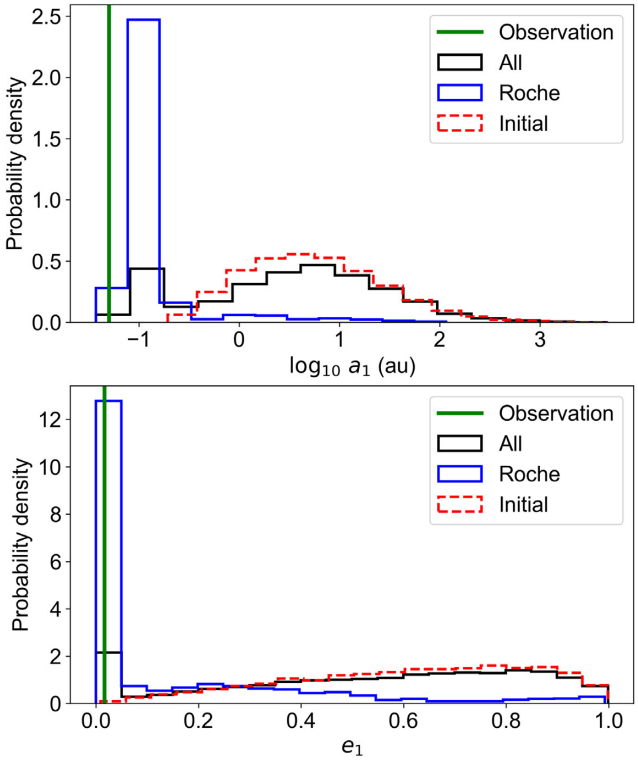

Figure 4. Inner binary orbit parameters. The top and bottom panels show the distribution for, respectively, the semimajor axis and eccentricity of the inner binary. Black lines show the final distribution for all systems, and blue lines show the final distribution for systems that crossed the Roche limit. Red dashed lines show the initial distribution for all systems, and the observed quantities (Gómez Maqueo Chew et al. 2012) are in green.

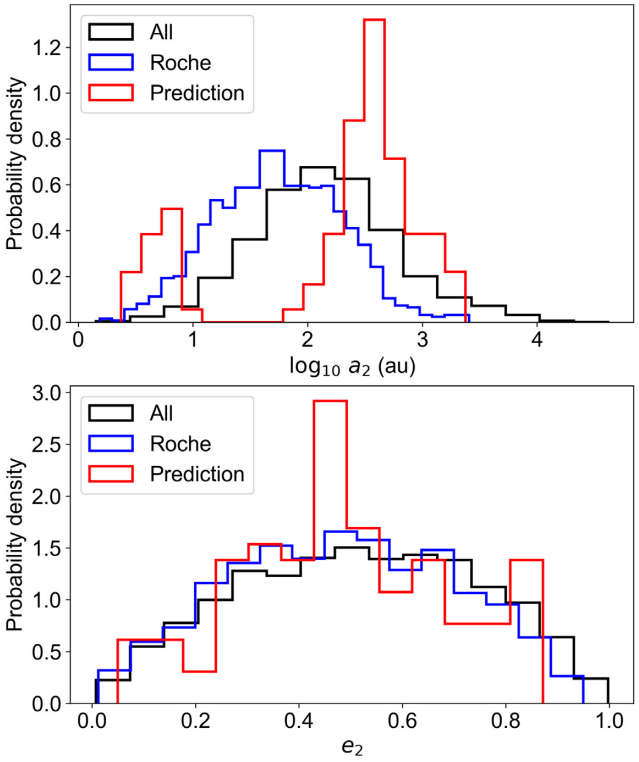

Figure 5. Outer binary orbit parameters. The top and bottom panels show the distribution for, respectively, the semimajor axis and eccentricity of the outer binary. Black lines show all systems, and blue lines show only systems that crossed the Roche limit. Red lines show Roche limit crossing systems constrained by the observed value for a_1. The cluster of constrained systems with $a_2 < 30$ au corresponds to $e_2 < 0.5$, and represents systems with a moderately tightened and circularized outer orbit.

Roche limit. Since we assume mass inversion, the fraction of binary mass transferred is constant between different systems. Realistically we may expect a constant mass transfer rate rather than constant fraction of binary mass transferred.

The time that the systems spend in each other Roche limit is about 1000 yr that results in a constant mass transfer rate of $\sim 6 \times 10^{-6}$ $M_\odot$ yr^{-1} (see Fig. 7). The Par 1802-like systems spend about a factor of 3 longer time inside the Roche limit, which results in a mass transfer rate of $\sim 3 \times 10^{-6}$ $M_\odot$ yr^{-1}. These mass transfer rates are not unreasonable to assume and we thus proceed with this proof-of-concept calculation. We note that alternative models exist (Sepinsky et al. 2007; Dosopoulou & Kalogera 2016; Hamers & Dosopoulou 2019) that incorporate orbital evolution, and will be included in future work.

5.2 Tidal heating

As the pre-main-sequence stars undergo mass transfer they also feel the tidal forces that shrink and circularized the orbit (see e.g. Fig. 3). The tidal model adopted throughout the three-body dynamical evolution followed the equilibrium tidal model from Hut (1980) that assumes a constant viscous time (e.g. Eggleton et al. 1998; Eggleton & Kiseleva-Eggleton 2001; Naoz 2016, see the latter for a complete set of equations). However, we are particularly interested in the response of the pre-main-sequence stars to the energy deposited within them due to tides during the Roche limit crossing period.

Tides on these polytropes that take orbital energy are transferred into heat in the star. This may cause the inflation of the star. Here we adopt a constant phase-lag tidal heating model (Goldreich & Soter 1966; Ferraz-Mello, Rodríguez & Hussmann 2008; Wisdom 2008), often used for brown dwarfs (e.g. Heller et al. 2010). Since the stars in questions did not begin their thermonuclear fusion reaction, this tidal model is adequate.[1] We note that the constant phase-lag model adopts a constant quality factor for each of the stars Q_j, with $j = 1$, 2. However, since a_1 and R_j of the stars ($j = 1, 2$) vary in time, the quality factor at the onset of Roche lobe crossing is dramatically different than the quality factor at the existing point. The evolution of Q strongly impacts the tidally driven orbital evolution of systems (Heller 2019).

For the following proof-of-concept calculation we adopt two quality factors to calculate the excess temperature due to tidal effects. First, we consider the relation between the quality factor and the viscous time:

$$Q_j = \frac{4}{3}\frac{k_1}{(1+2k_1)^2}\frac{Gm_j}{R_j^3}\frac{t_V}{n_1}, \tag{11}$$

from Naoz et al. (2016), with constant viscous time-scales $(t_V)_j = 0.5$ typical for M-dwarfs, classical apsidal motion constant

[1]Note that dynamical tides have a significant effect on tidal dissipation, and may allow more efficient tidal heating (see for review Mathis 2019). The tidal heating model used here is based on the static equilibrium tidal model and is sufficient for our proof-of-concept analysis.

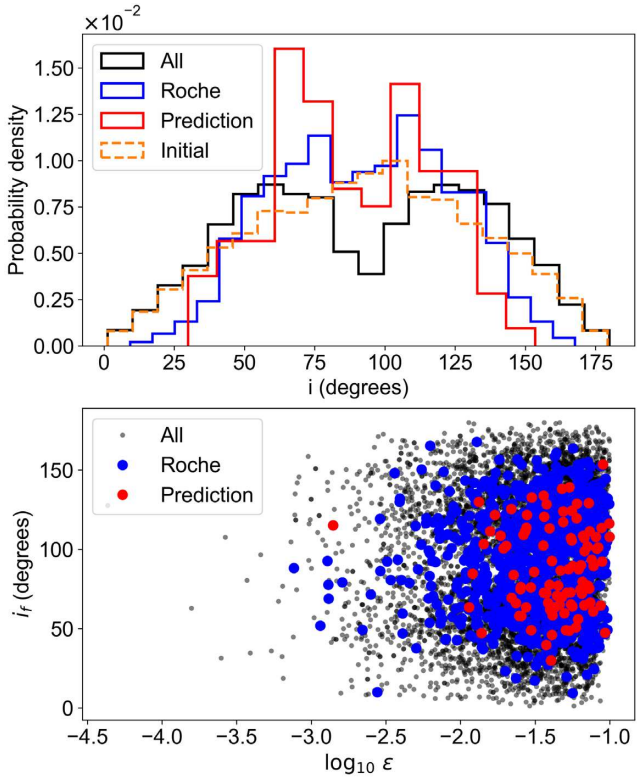

Figure 6. Inclination between inner and outer binary angular momenta, and ϵ. The top panel shows the distribution of the inclination, with blue marking all Roche limit crossing systems, dashed orange for the initial distribution for all systems, and red marking Roche limit crossing systems constrained by the observed value for a_1. The bottom panel shows the final inclination for all systems i_f as a function of ϵ, with all Roche limit crossing systems marked in blue, and Roche limit crossing systems constrained by the observed value for a_1 marked in red.

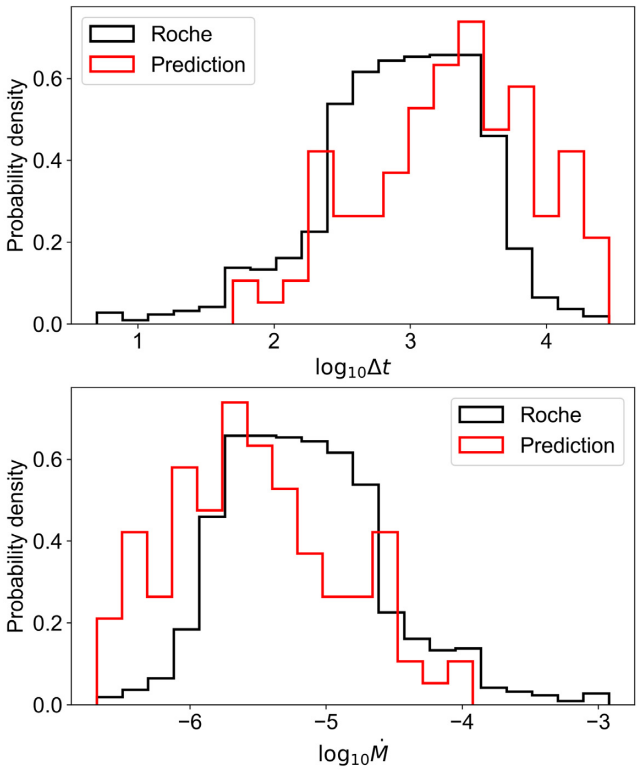

Figure 7. Mass transfer characteristics for Roche limit crossing systems. The top panel shows the amount of time Δt Roche limit crossing systems spent within the Roche limit, and the bottom panel shows the mass transfer rate for all Roche limit crossing systems determined using equation (10). Roche limit crossing systems constrained by the observed value for a_1 are marked in red.

$k_1 = 0.014$, and where the mean motion is $n_1 = 2\pi/P_1$. Since R_j and a_i varies in time, Q_j varies in time.

Tidal heating takes place throughout the tidal evolution. However, it is most significant when the stars are within each other Roche lobe regimes (see upper panel of Fig. 7 for time-scale). We thus limit ourselves to two relevant points in time of the evolution: the onset of the Roche limit, and exit from this regime. We find that for the majority of cases $Q_{j,\mathrm{enter}} \gg Q_{j,\mathrm{exit}}$, where the subscript 'enter' ('exit') refers to entering (exiting) the Roche limit. While tidal heating takes place for both stars, the 3 per cent mass difference results in slight changes in the amount of heating per unit mass, with the less massive star being heated more.

Under the tidal heating, constant phase-lag model, the potential of the less massive body is expressed in terms of periodic contributions of tidal frequencies at various phase lags (e.g. Heller et al. 2010), which can be expanded in terms of these phase lags. The phase lags $\epsilon_{\eta,j}$ for the jth body with $\eta = 0, 1, 2, 5, 8, 9$ are

$$Q_j\,\epsilon_{0,j} = \Sigma(2\Omega_{\mathrm{s},j} - 2n_1),$$

$$Q_j\,\epsilon_{1,j} = \Sigma(2\Omega_{\mathrm{s},j} - 3n_1),$$

$$Q_j\,\epsilon_{2,j} = \Sigma(2\Omega_{\mathrm{s},j} - n_1),$$

$$Q_j\,\epsilon_{5,j} = \Sigma(n_1),$$

$$Q_j\,\epsilon_{8,j} = \Sigma(\Omega_{\mathrm{s},j} - 2n_1),$$

$$Q_j\,\epsilon_{9,j} = \Sigma(\Omega_{\mathrm{s},j}), \tag{12}$$

with $\Sigma(x)$ defined as the algebraic sign of x:

$$\Sigma(x) = +1 \vee -1, \tag{13}$$

and $\Omega_{\mathrm{s},j}$ is the rotational period associated with the spin of the stars.

The change in orbital energy of star 1 due to star 2 (or vice versa) is then

$$\dot{E}_{\mathrm{orbit},j} = \frac{3k_{\mathrm{L}}Gm_l^2R_j^5}{8a_1^6}n\left(4\epsilon_{0,j} + e_1^2\left[-20\epsilon_{0,j} + \frac{147}{2}\epsilon_{1,j} + \frac{1}{2}[\epsilon_{2,j} - 3\epsilon_{5,j}] - 4\sin^2\psi_j[\epsilon_{0,j} - \epsilon_{8,j}]\right]\right), \tag{14}$$

where $j, l = 1, 2$, and the change in rotational energy is

$$\dot{E}_{\mathrm{rotation},j} = -\frac{3k_{\mathrm{L}}Gm_l^2R_j^5}{8a_1^6}\Omega_{\mathrm{s},j}\left(4\epsilon_{0,j} + e_1^2\left[-20\epsilon_{0,j} + 49[\epsilon_{1,j} + \epsilon_{2,j}] + 2\sin^2\psi_j[-2\epsilon_{0,j} + \epsilon_{8,j} + \epsilon_{9,j}]\right]\right), \tag{15}$$

where $k_{\mathrm{L}} = 0.5$ is the dynamical Love parameter and ψ_j is the obliquity of the jth body. All of the relevant variables are obtained through the dynamical evolution results described in Section 4.1, and the masses of the stars invert between Roche limit entry and

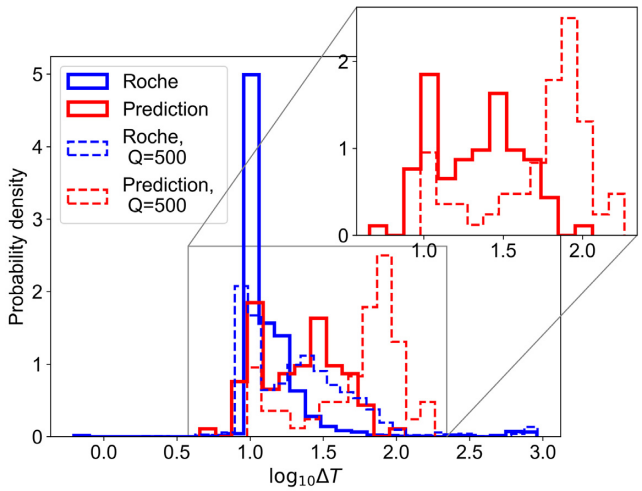

Figure 8. Temperature difference between inner binary stars. The solid lines show the temperature difference between the inner binary stars determined using equation (18) through the method detailed in Section 5.2. The quality factor adopted in this calculation follows equation (11), and varies with different a_1 and R_j. Roche limit crossing systems are in blue, and Roche limit crossing systems constrained by the observed value of a_1 are in red. The maximum ΔT for all Roche limit crossing systems is 910 K, and the maximum predicted ΔT for Roche limit crossing systems constrained by the observed value of a_1 is 115 K. Additionally, the temperature difference for an assumed constant quality factor $Q = 500$ is overplotted in dashed lines. With this constant Q, the maximum ΔT for all Roche limit crossing systems is 920 K. After constraining with the observed value of a_1, the maximum ΔT is 180 K.

exit (see Section 5.1). Finally, the change in total energy due to tides is

$$\dot{E}_j = -(\dot{E}_{\mathrm{orbit},j} + \dot{E}_{\mathrm{rotation},j}). \tag{16}$$

The temperature change for each body due to tidal heating is then evaluated from the Stefan–Boltzmann equation

$$dT_j = \left(\frac{\dot{E}_j/2}{4\pi R_j^2 \sigma_{\mathrm{SB}}} + T_{\mathrm{eff},j}^4 \right)^{1/4} - T_{\mathrm{eff},j}, \tag{17}$$

where σ_{SB} is the Stefan–Boltzmann constant, and $T_{\mathrm{eff},j}$ is the temperature at Roche-crossing for the jth body of mass m_j adopting Baraffe et al. (1998) model. We then estimate the above equation at two times: when the system enters and exits the Roche lobe regime.[2] In other words, $dT_j = dT_{j,\mathrm{enter}} + dT_{j,\mathrm{exit}}$, where subscript enter (exit) refers to entering (exiting) the Roche lobe regime. We note that $T_{j,\mathrm{eff}}$ at the entering and exiting points of the Roche limit are roughly the same because the short amount of time the stars spend in each other Roche lobe regime (see Fig. 7). The temperature difference is then estimated by

$$\Delta T = (dT_1 + T_{\mathrm{eff},1}) - (dT_2 + T_{\mathrm{eff},2}). \tag{18}$$

In Fig. 8, we show a histogram of the final excess temperatures as a result from the heuristic calculation of tidal heating. We find that Roche limit crossing systems have a wide range of ΔT, with a maximum $\Delta T_{\mathrm{max}} = 910$ K (Fig. 8). We predict a maximum $\Delta T_{\mathrm{predict}} \approx 115$ K.

The luminosity of the two stars is estimated by summing the total energy change due to tides for each star using equation (16) at entry and exit from the Roche limit. The luminosity difference between Par 1802-like stars (with a_1 within a factor of 2 from observation) has a median of $\sim 3 \times 10^{25}$ W, which is comparable to the observed luminosity difference of $\sim 7 \times 10^{25}$ W (Gómez Maqueo Chew et al. 2012).

Since the constant phase-lag tidal heating model typically adopts a constant Q, we complete a second set of calculations of ΔT for an assumed constant $Q = 500$. We predict a maximum $\Delta T \approx 180$ K for constant $Q = 500$. Both predictions ($\sim$115 K for Q following equation 11, and $\sim$180 K for constant $Q = 500$) are comparable to the observation of $\Delta T_{\mathrm{observed}} \approx 300$ K (Stassun et al. 2014). With $Q = 500$, the luminosity difference between Par 1802-like stars has a median of $\sim 5 \times 10^{26}$ W, comparable to observation.

6 DISCUSSION

The Par 1802 M-dwarf binary system is an interesting quandary for stellar evolution since one of the component stars has unexpectedly higher temperature compared to the other despite their almost identical (within 3 per cent) masses. Previous work by Stassun et al. (2014) and Gómez Maqueo Chew et al. (2012) have proposed that the temperature difference was caused by the presence of a third star. Here we focused on the dynamical evolution of such a system and have shown that observed quantities can be naturally reproduced. Furthermore, we predict the orbital configuration of such a tertiary companion.

We studied the secular evolution of the binary M-dwarf system Par 1802 in the presence of a third, far away star. We numerically solved the three-body hierarchical secular equation to the octupole level of approximation (i.e. the EKL mechanism; Naoz 2016). Tidal effects, GR precession, and pre-main-sequence evolution were self-consistently included in our simulations.

During the evolution, the EKL mechanism could cause large eccentricity excitations in the inner orbit, which prompted the inner binary to tighten and circularize (see top left-hand plot of Fig. 3). In some of these systems, eccentricity excitations caused the inner binary stars to cross their Roche limits (see Fig. 3). During that time, mass transfer could take place, resulting in the aforementioned temperature difference. As the stars' radii contracted their Roche-radii shrunk, effectively halting mass transfer, and the stars exit the Roche lobe regime.

We found that $\sim$15 per cent of all simulations were Roche limit crossing systems with the majority ($\sim$80 per cent) of these having circularized and their separation shrunk due to tides (see Fig. 4). We focused on systems that evolved to within a factor of 2 of the observed Par 1802 separation (of $\sim$0.05 au). These systems represented about 10 per cent of all Roche limit crossing systems, and about 1.5 per cent of all simulated systems. Since our initial conditions for semimajor axis and eccentricity featured broad distributions (with a_1 varying between $\sim$0.2 and 380 au and e_1 varying between $\sim$0.1 and 0.9), this 1.5 per cent fraction is statistically significant and suggests that systems similar to Par 1802 can exist in the presence of a tertiary companion.

For these systems similar to Par 1802, we constrain the orbital configuration for the Par 1802 tertiary star. In particular, we predict that the outer orbit is most likely to have a separation of 350 au (top panel of Fig. 5). We find that the predicted median eccentricity of the tertiary is $e_2 = 0.5$ (bottom panel of Fig. 5). The inclination (as

[2]In reality, heating takes place throughout the time the stars spend in the Roche limit. However, since we find that the maximum heating takes place when the stars exit their Roche limit, we evaluate heating only at these two points in time.

expected; e.g. Naoz & Fabrycky 2014) has a bimodal distribution with peaks centred around 70° and 110°.

During the time the system crossed its Roche limit, mass transfer took place and tidal heating was probably most efficient. The two stars of Par 1802 have an observed temperature difference of ∼300 K (Gómez Maqueo Chew et al. 2012). We conducted a proof-of-concept calculation, assuming conservative mass transfer during the Roche limit crossing time. For simplicity the two inner masses were set to be the observed masses, and thus, to match observations the mass ratio inverted over the course of the evolution. These assumptions determined the mass transfer rate (see Fig. 7). Following the Heller et al. (2010) tidal heating model we find about 0.2 per cent of all systems have temperature difference within a factor of 2 of the observed value. These systems represent a small fraction (5 per cent) of the Par 1802-like systems (i.e. systems with final inner binary separation within a factor of 2 of the observed separation). Since our mass exchange and tidal heating analysis are proof-of-concept and only accounts for heating at entry and exit from the Roche limit, we realistically expect a higher fraction of Par 1802-like systems to exhibit the observed temperature difference.

Finally, our results suggest that secular interaction in hierarchical triple-body systems, during their pre-main-sequence contractions, may lead to a generic feature: tight binaries with temperature difference. Par 1802 is a young system (∼2 Myr), which results in limited time for the EKL mechanism to operate. We thus expect similar, more pervasive behaviour for general triple systems. In particular, the presence of a tertiary star may explain the four other twin binaries with significant temperature differences discovered so far (Gómez Maqueo Chew et al. 2009, 2019; Wang et al. 2009; Gillen et al. 2017). This dynamically induced temperature difference may affect conclusions of the coevality of binary systems (e.g. Kraus & Hillenbrand 2009).

ACKNOWLEDGEMENTS

SJC would like to acknowledge the support of the Lau Endowment as part of the Undergraduate Research Scholars Program of the UCLA Undergraduate Research Center – Sciences, the Undergraduate Research Fellows Program, and the Maggie Gilbert Research Award through UCLA College Honors. SN thanks Howard and Astrid Preston for their generous support. We would like to thank Professor Stassun, Professor Gómez Maqueo Chew, Professor Heller, and Dr Hamers for their thoughtful comments and suggestions.

REFERENCES

Antonini F., Murray N., Mikkola S., 2014, ApJ, 781, 45
Auclair-Desrotour P., Mathis S., Le Poncin-Lafitte C., 2015, European Phys. J. Web Conf., 101, 04005
Baraffe I., Chabrier G., Allard F., Hauschildt P. H., 1998, A&A, 337, 403
Bataille M., Libert A.-S., Correia A. C. M., 2018, MNRAS, 479, 4749
Bergfors C. et al., 2010, A&A, 520, A54
Bode J. N., Wegg C., 2014, MNRAS, 438, 573
Braviner H. J., Ogilvie G. I., 2015, MNRAS, 447, 1141
Cargile P. A., Stassun K. G., Mathieu R. D., 2008, ApJ, 674, 329
Chabrier G., Baraffe I., 1997, A&A, 327, 1039
Dosopoulou F., Kalogera V., 2016, ApJ, 825, 71
Duquennoy A., Mayor M., 1991, A&A, 248, 485
Eggleton P. P., 1983, ApJ, 268, 368
Eggleton P. P., Kiseleva-Eggleton L., 2001, ApJ, 562, 1012
Eggleton P. P., Kiseleva L. G., Hut P., 1998, ApJ, 499, 853
Eggleton P. P., Kisseleva-Eggleton L., Dearborn X., 2007, in Hartkopf W. I., Guinan E. F., Harmanec P., eds, Proc. IAU Symp. 240, Binary Stars as Critical Tools & Tests in Contemporary Astrophysics. Cambridge Univ. Press, Cambridge, p. 347
Fabrycky D., Tremaine S., 2007, ApJ, 669, 1298
Fabrycky D. C., Johnson E. T., Goodman J., 2007, ApJ, 665, 754
Ferraz-Mello S., Rodríguez A., Hussmann H., 2008, Celest. Mech. Dyn. Astron., 101, 171
Fischer D. A., Marcy G. W., 1992, ApJ, 396, 178
Ford E. B., Kozinsky B., Rasio F. A., 2000, ApJ, 535, 385
Gillen E., Hillenbrand L. A., David T. J., Aigrain S., Rebull L., Stauffer J., Cody A. M., Queloz D., 2017, ApJ, 849, 11
Goldreich P., Soter S., 1966, Icarus, 5, 375
Gómez Maqueo Chew Y., Stassun K. G., Prša A., Mathieu R. D., 2009, ApJ, 699, 1196
Gómez Maqueo Chew Y., Stassun K. G., Prša A., Stempels E., Hebb L., Barnes R., Heller R., Mathieu R. D., 2012, ApJ, 745, 58
Gómez Maqueo Chew Y. et al., 2019, A&A, 623, A23
Greenberg R., 2009, ApJ, 698, L42
Griffin R. F., 2012, J. Astrophys. Astron., 33, 29
Guillochon J., Ramirez-Ruiz E., Lin D., 2011, ApJ, 732, 74
Hamers A. S., Dosopoulou F., 2019, ApJ, 872, 119
Heller R., 2019, A&A, 628, A42
Heller R., Jackson B., Barnes R., Greenberg R., Homeier D., 2010, A&A, 514, A22
Henry T. J., Jao W.-C., Subasavage J. P., Beaulieu T. D., Ianna P. A., Costa E., Méndez R. A., 2006, AJ, 132, 2360
Hut P., 1980, A&A, 92, 167
Janson M. et al., 2012, ApJ, 754, 44
Kiseleva L. G., Eggleton P. P., Mikkola S., 1998, MNRAS, 300, 292
Kozai Y., 1962, AJ, 67, 591
Kraus A. L., Hillenbrand L. A., 2009, ApJ, 704, 531
Lidov M. L., 1962, Planet. Space Sci., 9, 719
Liu S.-F., Guillochon J., Lin D. N. C., Ramirez-Ruiz E., 2013, ApJ, 762, 37
Mardling R. A., Aarseth S. J., 2001, MNRAS, 321, 398
Mathis S., 2019, EAS Publ. Ser., 82, 5
Moe M., Kratter K. M., 2018, ApJ, 854, 44
Mylläri A., Valtonen M., Pasechnik A., Mikkola S., 2018, MNRAS, 476, 830
Naoz S., 2016, ARA&A, 54, 441
Naoz S., Fabrycky D. C., 2014, ApJ, 793, 137
Naoz S., Farr W. M., Lithwick Y., Rasio F. A., Teyssandier J., 2013a, MNRAS, 431, 2155
Naoz S., Kocsis B., Loeb A., Yunes N., 2013b, ApJ, 773, 187
Naoz S., Fragos T., Geller A., Stephan A. P., Rasio F. A., 2016, ApJ, 822, L24
Perets H. B., Fabrycky D. C., 2009, ApJ, 697, 1048
Pribulla T., Rucinski S. M., 2006, AJ, 131, 2986
Raghavan D. et al., 2010, ApJS, 190, 1
Rappaport S., Deck K., Levine A., Borkovits T., Carter J., El Mellah I., Sanchis-Ojeda R., Kalomeni B., 2013, ApJ, 768, 33
Rose S. C., Naoz S., Geller A. M., 2019, MNRAS, 488, 2480
Salpeter E. E., 1955, ApJ, 121, 161
Sepinsky J. F., Willems B., Kalogera V., Rasio F. A., 2007, ApJ, 667, 1170
Shappee B. J., Thompson T. A., 2013, ApJ, 766, 64
Stassun K. G., Mathieu R. D., Cargile P. A., Aarnio A. N., Stempels E., Geller A., 2008, Nature, 453, 1079
Stassun K. G., Feiden G. A., Torres G., 2014, New Astron. Rev., 60, 1
Stephan A. P., Naoz S., Ghez A. M., Witzel G., Sitarski B. N., Do T., Kocsis B., 2016, MNRAS, 460, 3494
Thompson T. A., 2011, ApJ, 741, 82
Tokovinin A. A., 1997, Astron. Lett., 23, 727
Tokovinin A., Thomas S., Sterzik M., Udry S., 2006, A&A, 450, 681
Vick M., Lai D., 2018, MNRAS, 476, 482
Wang H. J., Wei J. Y., Shi J. R., Zhao J. K., 2009, A&A, 500, 1215
Wisdom J., 2008, Icarus, 193, 637
Witte M. G., Savonije G. J., 2002, A&A, 386, 222

This paper has been typeset from a TEX/LATEX file prepared by the author.